Analytic Solutions for Laser-Supported Combustion Wave Ignition above Surfaces

Anthony N. Pirri*
Physical Sciences Inc., Woburn, Mass.

Analytic solutions are presented for the time to plasma shielding above a laser-irradiated surface in an atmosphere. The time scale for ignition of a laser-supported combustion wave is determined as a function of laser intensity, material, spot size, and wavelength. The mechanism for absorption wave ignition involves surface vaporization, rapid heating of the target vapor and subsequent ignition in either the vapor or surrounding air. It is shown that over a range of intensities the vapor properties up to the time for ignition can be calculated by uncoupling the heating from the gas dynamics. The time history of the heating effects is obtained by doing a perturbation upon the flowfield. The flow is either one-dimensional planar or two-dimensional axisymmetric depending upon the ratio of an appropriate absorption time scale to a characteristic flow time. The one-dimensional planar analysis including the effects of unsteady surface vaporization is summarized, and the details of the two-dimensional analysis are presented. Results are compared with published computer solutions and existing experimental data for the time to plasma initiation above metal surfaces irradiated with 10.6 μ and 5 μ laser radiation.

I. Introduction

THE interaction of a high-power laser beam with surfaces in an atmospheric environment has been a subject of intensive study the past few years. In the intensity range up to 10^4 W/cm^2 most theoretical and experimental research has been devoted to determining the optical absorptivity and associated thermal response of surfaces as a function of laser wavelength. At 10.6 μ wavelength, and intensities $>10^4$ W/cm^2 the laser/surface interaction physics is dominated by the formation of a laser-supported absorption wave in either the vapor products or the air above the surface. Once the wave is initiated, a significant fraction of the incident laser intensity is attenuated and the resulting surface effects are altered. The thermal response of the surface material is affected by the high temperature plasma above the surface, and at laser intensities $>10^7$ W/cm^2 significant momentum may be transferred to the surface as a result of shock formation in the air.

Recently, Stegman et al.[1] and Klosterman and Byron[2] have presented experimental results for the initiation and propagation of laser-supported combustion waves above metals, ceramics and ablators that have been irradiated with a 10.6 μ laser. The laser pulse time was ≤ 5 msec with the peak intensity ranging from $10^4 - 2\times10^6$ W/cm^2. The observed combustion wave ignition was found to be strongly material dependent. It is apparent that for each material there is a distinct time scale for the initiation of absorption in either the vapor or the air. Whether or not a combustion wave is ignited depends on the magnitude of this time compared to the laser pulse time. The time history of the laser intensity that reaches the surface and the thermal response of the target then becomes a strong function of material. Thus, theoretical predictions of the target thermal response require a modeling of the combustion wave initiation in order to determine the energy flux incident upon the surface as a function of time.

Presented as Paper 76-23 at the AIAA 14th Aerospace Sciences Meeting, Washington, D. C., Jan. 26-28, 1976; submitted Feb. 5, 1976; revision received Aug. 6, 1976. The author would like to acknowledge J. Cronin who was responsible for the computer programming. This research was performed for the U.S. Naval Research Lab. through the Office of Naval Research under Contract N00014-74-0207. J.T. Schriempf of NRL was the contract monitor.

Index categories: Radiatively Coupled Flows and Heat Transfer; Lasers.

*Principal scientist. Member AIAA.

Thomas and Musal[3] have completed a theoretical study of the processes which lead to an absorbing vapor and subsequent combustion wave ignition in the adjacent air. They present a numerical solution for the case of a large diameter beam irradiating a surface. The time evolution of a one-dimensional layer of material as it evaporates and heats, until it becomes opaque to the laser radiation, is obtained by numerically solving the coupled equations of gas dynamics, absorption chemistry and radiative transfer. Their results indicate that an air combustion wave ignites immediately after a surface shielding vapor plasma is formed. Therefore, it can be assumed that the time to formation of an opaque vapor plasma is approximately equal to the time for ignition of a laser-supported combustion wave. Utilizing their computer code, Thomas and Musal have predicted[3] the time scale for combustion wave ignition above titanium surfaces under conditions corresponding to the experiments of Klosterman and Byron.[2] Calculations of the ignition time agree to within 20% of the experimental values. However, most of the time delay from laser on to plasma initiation is attributable to heating the surface to its vaporization temperature.

The purpose of this paper is to present analytic solutions for the time to vapor plasma shielding as a function of laser intensity, material, spot size and wavelength. It was shown previously[4] by this author that over a range of intensities the vapor properties up to the time for plasma ignition can be calculated by uncoupling the heating from the gas dynamics. The time history of the heating effects is obtained by doing a perturbation upon the flowfield. The flow is either one-dimensional planar or two-dimensional axisymmetric depending upon the ratio of an appropriate absorption time scale to a characteristic flow time. The one-dimensional planar analysis including the effects of unsteady surface vaporization and a time dependent laser intensity is carried out in Ref. 4, and analytic solutions are presented for the temperature history and vapor plasma ignition time. Assuming the laser-supported combustion (LSC) wave ignition time equals this time, we obtain results that are in good agreement with the numerical solutions of Thomas and Musal and agree adequately with the experimental data of Klosterman and Byron.[2] The present paper is directed toward further comparison of the 1D-theory with experiment and extension of the perturbation analysis to two dimensions. Thus, comparison of theory to experiment and prediction of plasma initiation times, when the vapor flow has become an axisymmetric jet

flow prior to ignition, is permitted. This is applicable to late time ignition of combustion waves at lower intensities, with smaller spot areas or above nonmetallic surfaces. In the next section the one-dimensional theory is summarized, and a comparison of the 1D theory with the latest step pulse data of Klosterman[5] is presented. Modifications of the vaporization model to obtain the conditions applicable to the two-dimensional vapor flow are discussed in Sec. III. Regions of unheated subsonic and supersonic jet flow as a function of absorbed laser flux are delineated. the perturbation analysis as applied to 2D initiation of absorption waves is then discussed and results and conclusions are presented in Sec. V.

II. Application of One-Dimensional Theory to Experimental Data

Review of 1D Theory

The approach taken to obtain analytic solutions for the time history of the evaporation, vapor heating and gas dynamic motion of both the vapor and air is as follows:[4] a simplified model for the vaporization of the surface in an air environment is formulated to provide the initial vapor properties shortly after the surface is heated to the vaporization temperature. The equations describing the coupled gas dynamics and radiative absorption are developed, and the parameters which govern the response of the vapor to laser heating are identified. These parameters are the following[4]

Unsteady Flow Parameter: $$f_1 = \frac{\delta}{a_i \tau_{ai}} \tag{1}$$

Two-Dimensional Flow Parameter: $$f_2 = \frac{\delta}{r_s} \tag{2}$$

Radiation Heating Parameter:

$$\Gamma_1 = \left(\frac{\theta_i}{2T_i}\right)\frac{\kappa_i \delta I_0}{\rho_i a_i^3} = \left(\frac{\theta_i}{2T_i}\right)\Gamma \tag{3}$$

where δ is a characteristic vapor dimension, a_i is the initial sound speed in the vapor, τ_{ai} is an absorption time scale estimated as[4]

$$\tau_{ai} = \left(\frac{2T_i}{\theta_i}\right)\frac{\rho_i c_v T_i}{\kappa_i I_0} \tag{4}$$

r_s is the spot radius, θ_i is the vapor ionization potential in units of temperature, κ_i is the initial vapor inverse Bremsstrahlung absorption coefficient, I_0 is the incident laser intensity, T_i is the initial vapor temperature, ρ_i is the initial vapor density and c_v is the vapor constant volume specific heat. Estimates of the magnitude of these governing parameters are made in Ref. 4. It is shown that, for the time period prior to the vapor becoming opaque, the heating process can be uncoupled from the gas dynamics over a significant range of laser intensities since $\Gamma_1 < 1$, and thus, $\Gamma \ll 1$. Under these conditions analytic solutions may be obtained for the time to vapor plasma initiation, as well as the vapor conditions until that time.

It is possible to map out regimes where approximate, analytic solutions to the plasma initiation problem may be obtained. An analytic solution map for aluminum is presented in Fig. 1. The interpretation of the delineated zones on the map proceeds as follows: first, Γ_1 can be shown to be dependent only upon I_s, the surface absorbed intensity ($I_s = \alpha_s I_0$, where α_s is the surface absorptivity). Therefore, a horizontal line can be drawn at the intensity level where $\Gamma_1 = 1$. Below this line the heating can be considered to be a perturbation upon the fluid mechanics. Similarly, f_1 is a function only of I_s, and a horizontal line can be drawn where $f_1 = 1$. For the chosen definition of $\delta = u_i \tau_{ai}$, where u_i is the initial vapor velocity, the flow can be considered steady at absorbed intensities below this line. Lines where $f_2 = 1$ for $r_s = 1$ cm and $r_s = 10$ cm are also drawn. To the left of each respective line are regimes of one-dimensional flow while to the right the flow is two-dimensional. To determine which region on the map is appropriate for a particular case, the line of $I_s = F(\tau_{ai})$, which results from Eq. (4) and $I_s = \alpha_s I_0$, is drawn. Each case lies on a point along this line. For example, at $I_s = 10^5$ W/cm^2, $\tau_{ai} = 1.98 \times 10^{-5}$ sec for aluminum. This corresponds to point A on Fig. 1 and lies in the region of one-dimensional steady flow with perturbation heating. It should be noted that τ_{ai} in Fig. 1 has been labeled as the pulse time required to initiate, since no absorbing plasma would be expected for pulse times less than this value.

The analytic solution obtained for the case of planar one-dimensional flow is applicable when the beam radius is much larger than a characteristic vapor layer dimension. Results for the vapor temperature until plasma ignition and the characteristic time for ignition are obtained by performing a perturbation analysis in Γ on the vapor flow equations.[4] The results for the vapor temperature and plasma initiation time scale, when the vaporization rate is a constant in time, are

$$T = T_i \left\{ 1 + \Gamma \ln \left[1 - \frac{\Gamma\theta_i}{2T_i} \frac{\exp(-\kappa_i u_i t)}{\kappa_i \delta M_i \left[\frac{5}{2\delta} + \frac{M_i^2}{1 - M_i^2 \delta}\right]} \left(e^{\kappa_i x} - 1\right) \right] - \frac{2T_i}{\Gamma\theta_i} \right\} \tag{5}$$

and

$$\tau_a = \tau_{ai}\left[\frac{5}{2\gamma} + \frac{M_i^2}{1 - M_i^2 \delta}\right] 2T_i/\theta_i \Gamma \tag{6}$$

where M_i is the initial vapor flow Mach number, γ is the vapor specific heat ratio, u_i is the initial vapor flow velocity and x is the position in the vapor layer referenced from the surface. When the vaporization rate is nonsteady, the expressions are more complicated and a quadrature integration must be performed to obtain the ignition time.[4]

A calculation was performed to compare with the sample case computer solution of Thomas and Musal.[3,4] For this case a 10.6 μ laser beam of intensity $I_0 = 2 \times 10^6$ W/cm^2 irradiates an aluminum surface. Thomas and Musal assume $\alpha_s = 0.15$

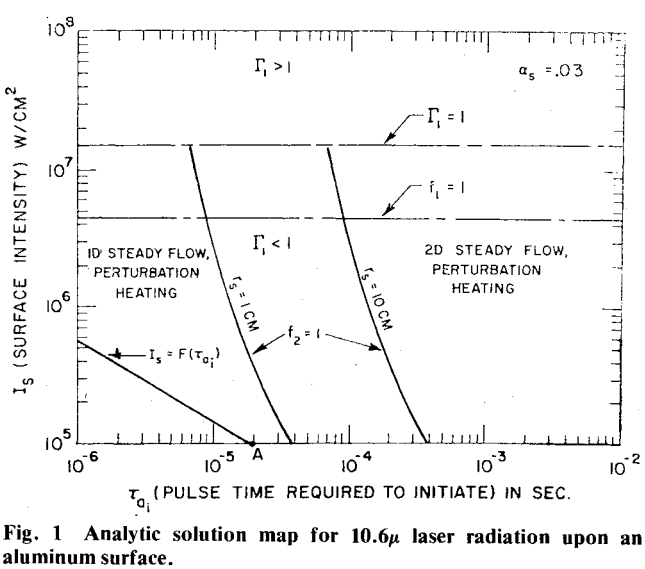

Fig. 1 Analytic solution map for 10.6μ laser radiation upon an aluminum surface.

after vaporization begins, and the intensity is a step function in time. Using an effective surface absorptivity prior to vaporization, they also calculate the time to raise the surface to the vaporization temperature, $\tau_v = 1.98 \times 10^{-4}$ sec. The material constants for aluminum plus $\alpha_s = 0.15$ and $I_0 = 2 \times 10^6$ W/cm^2 can be substituted into the vaporization model of Ref. 4 to obtain the initial vapor properties as a function of time. The numerical values of the dominant parameters based on the steady-state vapor properties become

$$a_i = 1.26 \times 10^5 \text{cm/sec}$$

$$\rho_i = 5 \times 10^{-4} \text{gms/cm}^3$$

$$T_i = 3080^\circ \text{K}$$

$$u_i = 4.43 \times 10^4 \text{cm/sec}$$

$$\kappa_i = 2 \times 10^{-3} \text{cm}^{-1}$$

$$\tau_{ai} = 8.49 \times 10^{-6} \text{sec}$$

$$\delta = 0.376 \text{cm}$$

$$\Gamma = 0.0277$$

Since $\tau_{ai} \ll 800$ μ sec, which is the time for the vaporization rate to reach its steady-state value, unsteady vaporization effects must be included as indicated in Ref. 4. The time for the onset of plasma shielding is obtained by numerically satisfying the requirement of the unsteady vaporization version[4] of Eq. (6). The result for the ignition time τ_{ig} (since the onset of vaporization) is

$$\tau_{ig} = \tau_a = 55\mu \text{ sec}$$

as compared to the absorption time deduced from the computer solution

$$\tau_{ig}(\text{Ref. 3}) \approx 50\mu \text{ sec}$$

The temperature profiles obtained using Eq. (5) are compared to the results of Ref. 3 at the time $t = \tau_{ig}$ in Fig. 2. Thomas and Musal began their calculation with an initial thickness equal to 0.2 cm. Their code is started at $t = 2.23 \times 10^{-4}$ sec so the vaporization rate is allowed to build up for 25 μsec. This incubation time is attributed to the coalescence of waves in the flow to form the air shock. Plasma shielding begins when $t = \tau_v + \tau_{ig} = 2.48 \times 10^{-4}$ sec, and the temperature profile in the vapor at this time is indicated by the circles in Fig. 2. The analytic profile is obtained from Eq. (5) with time dependent values for the vapor properties.[4] The vaporization rate was allowed to build up to 25 μsec and the profiles were computed beginning at $t = 2.23 \times 10^{-4}$ sec. The analytic result for the temperature profile at the onset of plasma shielding $t = \tau_{ig} + \tau_v = 2.53 \times 10^{-4}$ sec is the solid line. Thus, the analytic results are in good agreement with the computer solution.

Application of Theory to Recent MSNW Data

Recently Klosterman[5] has obtained experimental data for the time to laser-supported combustion wave initiation (after vaporization has started) for 10.6μ and 5μ laser pulses irradiating aluminum and titanium foils. The laser was equipped with an explosive shutter which allowed the laser intensity to build up before the target was irradiated. Thus, the target sees essentially a step laser pulse (rise time 100-200 μsec) of up to 4 msec in duration. the spot radius ranged from 0.25 cm to 1 cm. The initiation time was measured using both a photodiode, plus spectroscopy to detect vapor emission, and streak photographs.

The heating characteristics of the foil determine whether the vaporization proceeds at a steady or unsteady state. The titanium foils utilized in the experiments were of 1 mil thickness. The thermal diffusivity of the titanium is approximately 0.06 cm^2/sec and therefore, the estimated time to diffuse the thickness of the titanium foil is approximately 125 μsec. Since this is of the order of the observed ignition time, thermal conduction is important during vaporization, and the vaporization rate is a function of time. For aluminum, the thermal diffusivity is approximately 0.7 cm^2/sec. The time to diffuse the thickness of the foil is 9 μsec. Observed ignition times are much greater than this time so the foil heats uniformly. Thermal conduction in the foil is unimportant and vaporization proceeds at a steady rate.

A summary of Klosterman's experimental results for the time to plasma initiation, *after vaporization begins*, above an aluminum surface irradiated with a 10.6μ laser pulse is presented in Fig. 3. The laser intensity was changed primarily by varying the spot radius. The theoretical results from the one-dimensional model of Ref. 4 are also shown in Fig. 3. It is assumed, hereafter, that the vapor plasma ignition time equals the LSC wave ignition time. The theoretical results are presented for steady-state evaporation, and the surface absorptivity α_s is taken to be 0.15. The largest uncertainty in the initiation theory is the value of the elastic collision cross section for aluminum vapor that is inserted directly into the relation for the inverse Bremsstrahlung absorption coefficient. Thomas[3] uses the value for this cross section $\sigma = 20\pi a_0^2$ where a_0 is the Bohr radius. The model of Hyman and Kivel[6] for the neutral-electron inverse Bremsstrahlung absorption coefficient of highly polarizable atoms yields $\sigma = 50\pi a_0^2$, and their results for the alkali atoms, when compared to more detailed calculations, tend to be low in the temperature range of interest. Results shown in Fig. 3 indicate that the theoretical predictions are sensitive to the value of this cross section; however, when the aforementioned values are utilized, reasonable agreement with the data is obtained.

The theoretical results for titanium are shown along with the experimental data in Fig. 4. The surface absorptivity α_s is taken to be 0.25 and the elastic collision cross section is taken as $\sigma = 30\pi a_0^2$. This cross-section value is that used by Thomas; however, the model of Hyman and Kivel again predicts a significantly higher value. Results are presented for 10.6 μ and 5 μ, and the model predicts a slightly less than λ^{-2} dependence upon the ignition time, where λ is the laser wavelength. The vaporization rate is unsteady. Since at 10.6μ the vaporization rate is lower at the time of ignition than for the 5 μ case, ignition occurs slightly sooner at 5 μ than would be predicted by simple λ^{-2} scaling.

The time to vaporization for these foils was of the order of a millisecond. Therefore, at the lower intensities ($\approx 10^5$ W/cm^2) the ignition times were of the order of the time to vaporization. This was not the case in Refs. 2 and 3. Although the theoretical results of the one-dimensional model yield reasonable agreement with these data, the uncertainty in the

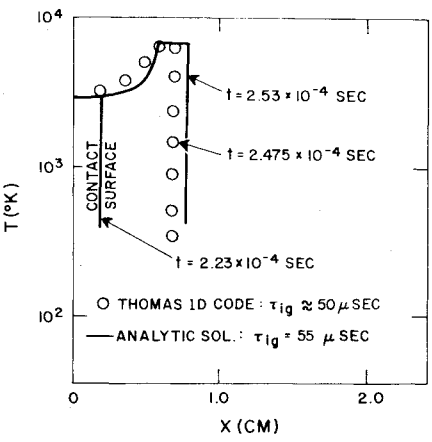

Fig. 2 Analytic solution for temperature profile in aluminum vapor prior to onset of plasma shielding, and comparison with computer solution of Thomas and Musal.[3]

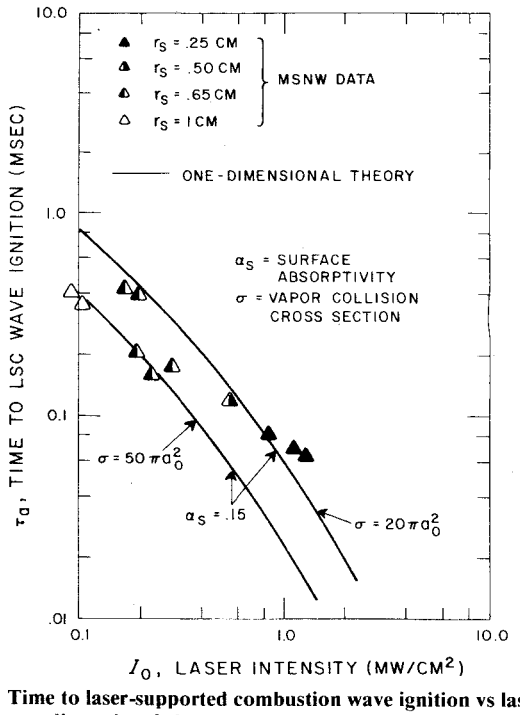

Fig. 3 Time to laser-supported combustion wave ignition vs laser intensity: one-dimensional theory results and comparison with data of Klosterman[5]; 10.6μ, aluminum surface and steady-state vaporization.

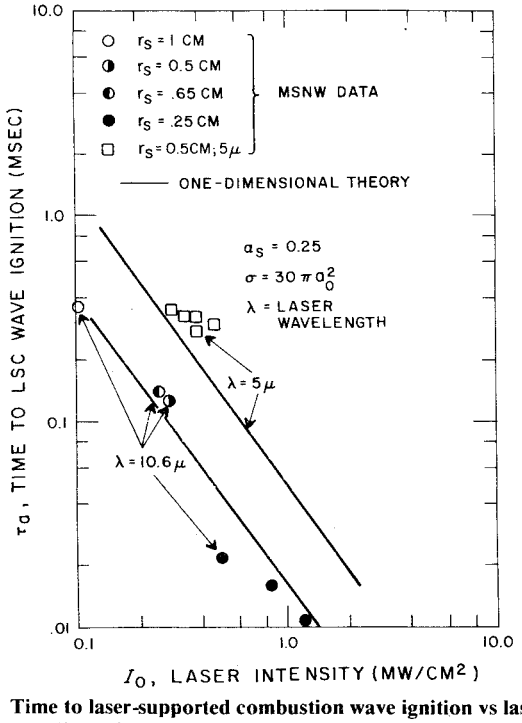

Fig. 4 Time to laser-supported combustion wave ignition vs laser intensity: one-dimensional theory results and comparison with data of Klosterman[5]; 10.6μ and 5μ, titanium surface and unsteady vaporization.

cross sections and applicability of the one-dimensional initiation model to these data must be addressed. The spot sizes are fairly small and we must compute the time for sound waves to propagate across the vapor jet along with the thickness of the vapor layer compared with the spot size. This will indicate the importance of two-dimensional effects on the flow. The uncertainty in the cross sections can only be accounted for by making calculations with the best estimates of these cross sections and examining the sensitivity of results to these estimates. The sound speed in the vapor for both cases is approximately 10^5 cm/sec. Therefore, sound waves propagate across the vapor layer parallel to the surface in time scales $< 10^{-5}$ sec. Therefore, two-dimensional effects should be affecting the flow. In addition, the layer thickness is $\approx 1-2$ cm when ignition occurs. Thus, it appears that two-dimensional spreading effects should be included in studies of LSC wave ignition for the conditions of these experiments.

III. Formulation of Two-Dimensional Analysis

Introduction

In Sec. II and Ref. 4 it was noted that the one-dimensional plasma initiation theory should be valid provided the thickness of the vapor layer does not become greater than a spot radius prior to ignition. This is strictly valid only when the velocity of the vapor is close to the sound speed. Information across the vapor layer is transmitted at the speed of sound, and the effects of a finite spot diameter are communicated to the axis of symmetry in a time scale equal to the spot radius divided by the sound speed in the vapor. When the time to absorption wave initiation is much greater than this time, two-dimensional effects of vapor expansion are important. This would be expected at intensities much less than 10^6 W/cm^2 and for spot radii of the order of 1 cm or less. Ablators tend to vaporize profusely,[1] and when absorption wave ignition occurs, it occurs in the vapor jet flow field. A two-dimensional analysis is required to predict ignition times under these conditions. In addition, the time scale for ignition can be written

$$\tau_a = \frac{1}{\lambda^2}\bar{K}F(\lambda T)$$

where $\bar{K}$ is a complicated function that accounts for the flow effect and $F(\lambda T)$ is a weak function of wavelength and temperature. It can be seen from Eq. (7) that as you decrease the wavelength, the ignition time increases approximately as the square of the wavelength for constant flow effects. The longer ignition time scale for lower wavelengths implies that two-dimensional effects will become more important at wavelengths less than 10.6 μ.

Unheated Vapor Dynamics Modeling

The first step in modeling the two-dimensional effects on absorption wave initiation is to determine the dynamics of the unheated vapor flow field. The configuration of the 2D flow field will depend strongly upon: 1) the stagnation pressure to static pressure ratio in the vapor at the surface, 2) the ratio of the initial vapor pressure to the ambient pressure, and 3) the vapor Mach number at the surface. The values of these properties *at the surface* can only be determined by suitably modifying the one-dimensional surface vaporization model of Ref. 4. This is done as follows:

The 1D vaporization model applies when the pressure in the vapor is sufficiently greater than the ambient pressure to create an air shock.[4] The air shock matching condition relates the vapor velocity and pressure, and the relation for the vapor velocity becomes

$$u = \frac{a_\infty}{\gamma_\infty}\left(\frac{p_v}{p_\infty} - 1\right)\sqrt{\frac{2\gamma_\infty/(\gamma_\infty+1)}{\frac{p_v}{p_\infty} + \frac{(\gamma_\infty-1)}{(\gamma_\infty+1)}}} \tag{8}$$

where u is the vapor velocity, p_v is the pressure in the vapor, and a_∞, γ_∞ and p_∞ are the ambient sound speed, specific heat ratio and pressure, respectively. When the vapor flow begins to go two-dimensional, Eq. (8) must be appropriately replaced to determine the vapor properties at the surface. The relation to be utilized in place of Eq. (8) is a function of the laser in-

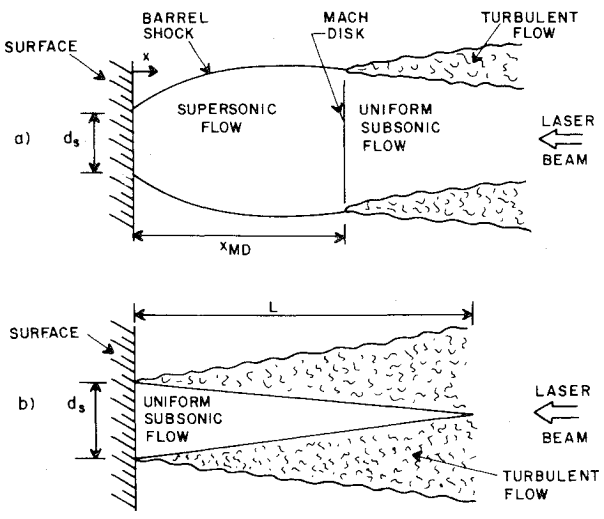

Fig. 5 Structure of two-dimensional jet flow: a) supersonic jet, b) subsonic turbulent jet.

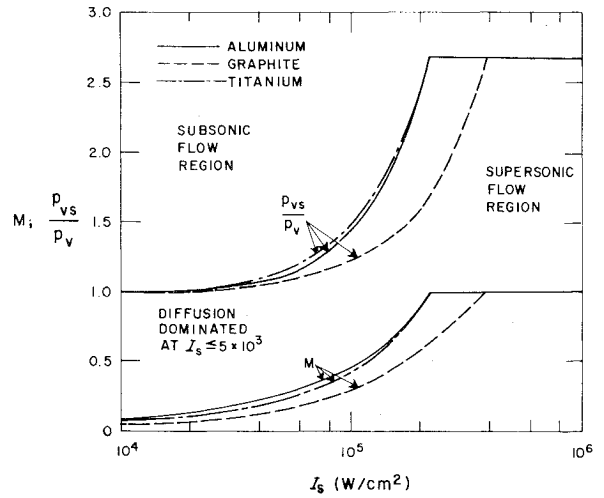

Fig. 6 Vapor properties at the surface vs absorbed laser intensity and two-dimensional flow regimes.

tensity. Depending upon the intensity, the modeling of the two-dimensional vapor flow can be divided into two regimes: 1) $p_v > p_\infty$ and $p_{vs}/p_v = (\gamma_v + 1)$ where p_{vs} is the vapor stagnation pressure and γ_v is the vapor specific heat ratio; and 2) $p_v = p_\infty$ and $p_{vs} > p_\infty$. In each of these regimes the vapor flow field is dominated by different phenomena, and the laser intensity will determine which flow effects control the ignition process. The two regimes are illustrated in Fig. 5.

When $p_v > p_\infty$, the inviscid flowfield is controlled by the ratio of the dynamic pressure at the surface to the ambient pressure. For this case the dynamic pressure in the vapor will be significantly higher than the ambient pressure. Once the flow begins to go two-dimensional, waves send information back to the surface causing the flow to accelerate until it chokes at the surface. After the transient period has subsided, a steady flow is established where the vapor velocity becomes sonic at the surface. The one-dimensional model is modified to get the surface vapor properties for the two-dimensional jet flowfield by replacing Eq. (8) by the condition that at the surface $u = a$, where a is the sound speed in the vapor. After the vapor leaves the vicinity of the surface, it expands supersonically. Because the flow tends to over-expand, a Mach disk forms and shocks the vapor back to ambient pressure (cf. Fig. 5a). A barrel shock forms the pressure boundary between the edges of the vapor jet and the ambient air.

As the laser intensity is decreased, the pressure in the vapor decreases until $p_v = p_\infty$. When $p_v = p_\infty$, and the laser intensity is decreased further, the vapor velocity can no longer remain sonic at the surface. The vapor flowfield becomes that of a subsonic turbulent jet with an inviscid inner core (Fig. 5b). The vapor pressure remains equal to the ambient pressure, and the vapor velocity at the surface decreases as the laser intensity is decreased. The surface vaporization model is modified by replacing Eq. (8) by the relation $p_v = p_\infty$ in the vapor.

The above descriptions of the vapor flowfield are valid provided 1) the time to absorption wave ignition is sufficiently long that a two-dimensional steady flow is established, and 2) the vapor velocity remains large so that the effects of vapor/air molecular diffusion are negligible in the jet core. Diffusion becomes important when the air/vapor mixing region is approximately equal to the thickness of the vapor layer; i.e.

$$ut \approx \sqrt{\mathfrak{D}t} \tag{9}$$

where t is time since evaporation has begun and D is the molecular diffusion coefficient. From Hirschfelder, Curtiss and Bird[7] a rigid sphere model yields the expression for the diffusion coefficient

$$D = 2.6280 \times 10^{-3} \frac{(T^3/\bar{M})^{1/2}}{p\bar{\sigma}^2} \tag{10}$$

where p is the pressure in atm of the mixture of vapor and air, T is the temperature, $\bar{M}$ is the mean molecular weight of the mixture and $\bar{\sigma}$ is the mean molecular diameter. For a mixture of aluminum vapor and air at 2500 K, using Eq. (10), we obtain $D \approx 6$ cm^2/sec. For a titanium vapor/air mixture at 3500 K, we obtain $D \approx 7$ cm^2/sec. Observed combustion wave ignition occurs during time scales of approximately $10^{-6} - 10^{-4}$ sec after vaporization begins. Substituting into Eq. (9), we obtain the result that for aluminum vapor/air and titanium vapor/air mixtures, molecular diffusion becomes important when $\mu < 2.5 \times 10^3$ cm/sec.

Two-Dimensional Flow Configuration Regimes

Using the surface vaporization model, described in Ref. 4 and appropriately modified as indicated above, we can obtain the vapor properties at the surface and the two-dimensional flow configuration regimes as a function of laser intensity. Results for aluminum, titanium and graphite vapor are presented in Fig. 6. The following properties are presented in Fig. 6 as a function of surface absorbed laser intensity; Mach number at the surface (M), and ratio of the vapor stagnation pressure to static pressure at the surface (p_{vs}/p_v). It can be seen in Fig. 6 that the properties of the evolved vapor lead to supersonic jetting when the surface absorbed intensity is greater than 2×10^5 W/cm^2 for titanium and aluminum. For graphite, supersonic jetting results when the absorbed intensity is greater than 5×10^5 W/cm^2. At intensities below these values the vapor jet remains a subsonic turbulent jet when the time scale is sufficiently long that a 2D steady flowfield forms. Molecular diffusion effects and mixing of the vapor and air in the jet core do not dominate the flow configuration until the absorbed intensity is much less than 10^4 W/cm^2.

In order to calculate the requirements for LSC wave ignition utilizing the perturbation analysis, it is necessary to model the entire unheated vapor flowfield. The vapor properties at the surface are computed as previously indicated. The remainder of the flowfield is described by using appropriate supersonic and subsonic jet models.

Supersonic Jet Model

The supersonic flow configuration is illustrated in Fig. 5a. The structure of an underexpanded supersonic jet has been

studied extensively. One of the earliest models for the jet boundary profile and Mach disk location was proposed by Adamson and Nicholls.[8] The results of their analysis and subsequent experimental and theoretical studies by many authors[9] indicate that the position of the Mach disk is given to good accuracy by

$$x_{MD}/d_s = 0.67(p_{vs}/p_\infty)^{1/2} \tag{11}$$

where x_{MD} is the distance from the surface to the Mach disk, and d_s is the initial jet diameter which equals the laser beam diameter at the surface. For example, if an aluminum target is irradiated such that the surface absorbed intensity $I_s \approx 4\times10^5$ W/cm^2, the previous models yield the result $p_{vs}/p_\infty \approx 5$ and $x_{MD}/d_s \approx 1.5$.

The actual flowfield properties from the surface to the Mach disk are computed by using the model of Adamson and Nicholls for the jet boundary configuration, and applying quasi-one-dimensional nozzle flow theory[10] to obtain the flowfield variables between the surface, $x=0$, and x_{MD}. The supersonic jet is treated as a quasi-one-dimensional nozzle, and the local Mach number is related to the jet area by integrating the expression

$$\frac{dM^2}{M^2} = \frac{2(1+\frac{\gamma_v-1}{2}M^2)}{(1-M^2)}\frac{dA}{A} \tag{12}$$

where $A=A(x)$ is the local jet area, $M=M(x)$ is the local jet Mach number, and x is measured from the surface (cf. Fig. 5a). $A(x)$ is obtained from the jet boundary configuration. Once the Mach number as a function of x has been calculated, the pressure and temperature in the vapor jet from the surface to the Mach disk is computed from the isentropic relations[10]

$$\frac{p}{p_{vs}} = (1+\frac{\gamma_v-1}{2}M^2)^{-\gamma_v/(\gamma_v-1)} \tag{13}$$

$$\frac{T}{T_s} = (1+\frac{\gamma_v-1}{2}M^2)^{-1} \tag{14}$$

where p and T are the local pressure and temperature in the vapor jet. Example results for the vapor properties out to the Mach disk when $I_s \cong 4\times10^5$ W/cm^2 upon an aluminum surface are presented in Fig. 7. The ratios p/p_{vs} and T/T_s along with the local Mach number are plotted as a function of x/d_s.

The strength of the Mach disk is determined by the condition that the vapor must be shocked to ambient pressure. In Fig. 7 the results downstream of the Mach disk are for $p_\infty = 1$ atm. The flow downstream of the Mach disk is uniform flow until turbulent diffusion from the edges of the jet cools the vapor and decreases the velocity to zero. This part of the supersonic jet configuration resembles a subsonic turbulent jet.

Subsonic Jet Model

The subsonic flow configuration is illustrated in Fig. 5b. The Reynolds number based upon the spot radius, $d_s/2$, is approximately 2000-4000 for the conditions specified in Fig. 6. Subsonic jet flow corresponding to these Reynolds numbers is turbulent, and the structure of the jet consists of a conical inner core of uniform flow surrounded by a growing turbulent flow region.[11] The length of the uniform flow inner core, L, is approximately nine times the spot radius r_s, and the ratio L/r_s is constant.[11] This results because the rate at which turbulence diffuses inward from the edges of the jet is proportional to the flow velocity. The thickness of the turbulent region $\delta \sim (\nu_T x/U)^{1/2}$ where U is the mean flow velocity and ν_T is an effective turbulent kinematic viscosity. When a mixing length hypothesis for the turbulent flow is invoked, ν_T can be considered proportional to the product of a mean flow velocity and a length scale. Therefore, δ/x becomes independent of flowfield variables. When $\delta = r_s$, $x=L$, and it is concluded that L/r_s is approximately a constant independent of the flow rate.

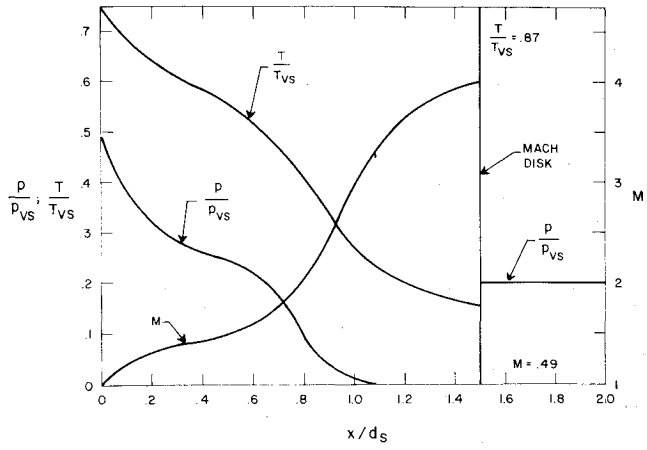

Fig. 7 Unheated supersonic jet properties vs x/d_s; aluminum surface and $I_s \cong 4\times10^5$ W/cm^2.

Downstream of the inner core region the mean flow velocity and temperature $\sim 1/x$ once the turbulence has become fully developed.[11] Although a detailed description of the flowfield is necessary before the perturbation analysis can be applied, it will be shown in the Sec. IV that ignition can only occur in the uniform flow core region. Once the flow begins to cool due to turbulent diffusion, LSC wave ignition is no longer possible.

IV. Perturbation Technique Applied to Jet Flow

Formulation for Supersonic Jet Flow

The supersonic jet can be divided into three parts. From the surface to the Mach disk the flowfield is treated as a quasi-one-dimensional nozzle flow. Downstream of the Mach disk the flow is subsonic, and the conditions are uniform until the turbulence diffuses to the centerline from the edges of the jet. The uniform flow forms a jet inner core similar to the subsonic jet case. Finally, turbulence dissipates and cools the jet flowfield. The perturbation technique is first applied to the supersonic flow region from the surface to the Mach disk.

Consider the quasi-one-dimensional description of the expanding flow. The equations describing the steady flowfield can be written

$$\frac{d}{dx}(\rho UA) = 0 \qquad \text{(continuity)} \tag{15}$$

$$u\frac{du}{dx} = -\frac{1}{\rho}\frac{dp}{dx} \qquad \text{(momentum)} \tag{16}$$

$$\rho u\frac{d}{dx}(h+\frac{u^2}{2}) = \kappa_\nu I \qquad \text{(energy)} \tag{17}$$

where ρ is the local vapor density, u is the velocity, A is the local jet area, p is the local pressure in the vapor, h is the local enthalpy, κ_ν is the local inverse Bremsstrahlung absorption coefficient and I is the local value of the radiation intensity. Equations (15)-(17) are made dimensionless in the following way

$$\hat{x} = \frac{x}{r_s},\ \hat{u} = \frac{u}{a_i},\ \hat{p} = \frac{p}{\rho_i a_i^2},\ \hat{\rho} = \frac{\rho}{\rho_i},$$

$$\hat{h} = \frac{h}{a_i^2},\ \hat{A} = \frac{A}{A_s},\ \hat{\kappa}_\nu = \frac{\kappa_\nu}{\kappa_{\nu_i}},\ \hat{I} = \frac{I}{I_0} \tag{18}$$

where A_s is the laser beam area at the surface corresponding to a beam radius r_s, ρ_i is the initial vapor density at the surface, κ_{ν_i} is the initial value of the absorption coefficient, I_0 is the laser intensity, and a_i is the initial vapor sound speed (see Ref. 4). The resulting equations become dimensionless and are identical to Eqs. (15)-(17) except for the energy equation which becomes

$$\rho u \frac{d}{dx}\left(h+\frac{u^2}{2}\right)=\Gamma\kappa_\nu I \tag{19}$$

where all quantities are now dimensionless (the hats have been dropped for convenience, and Γ is the radiation heating parameter[4]

$$\Gamma=\frac{\kappa_{\nu_i} r_s I_0}{\rho_i a_i{}^3} \tag{20}$$

Since $\Gamma \ll 1$ (Sec. II), all variables are expanded in Γ, and the resulting differential equations can be solved to increasing order in Γ. However, the introduction of a varying area contour suggests the reduction of Eqs. (15)-(19) to one differential equation for the Mach number as a function of position. First, an equation of state is added so that

$$h=\frac{\gamma_v}{\gamma_v-1}\frac{p}{\rho}=\frac{a^2}{\gamma_v-1} \tag{21}$$

where a is the sound speed. Combining the dimensionless version of Eqs. (15) and (16), (19) and (21), and after much algebra,[12] we obtain

$$\frac{(M^2-1)}{M^2\left[1+\frac{M^2(\gamma_v-1)}{2}\right]}\frac{dM^2}{dx}+\frac{1}{F}\frac{dF}{dx}(1+\gamma_v M^2)=\frac{2}{A}\frac{dA}{dx} \tag{22}$$

where M is the local Mach number and

$$\frac{dF}{dx}=\frac{\Gamma\kappa_\nu AI}{W}$$

$$W=\rho u A=\text{const.} \tag{23}$$

Each of the dependent variables in Eqs. (22) and (23) is expanded in powers of Γ. Therefore,

$$M=M_0+\Gamma M_1+\ldots$$

$$I=I_0+\Gamma I_1+\ldots$$

$$\text{etc.} \tag{24}$$

The variable κ_ν is expanded in Γ after the exponential dependence of the absorption coefficient upon temperature is extracted since only slowly varying functions are expanded in powers of the radiation heating parameter.[4] After expanding the dependent variables as indicated above and substituting into Eq. (22), we obtain to first order in Γ

$$(M_0^2-1)\frac{d(M_0M_1)}{dx}+M_0M_1\frac{dM_0{}^2}{dx}$$

$$=-\frac{(\gamma_v-1)}{2a_0{}^2}\frac{\kappa_{\nu_0}I_0A}{W}M_0^2(1+\gamma_v M_0^2)e^{[(\theta_i/2T_0)\Gamma T_1)]}$$

$$+\left\{2M_0M_1\left[1+\frac{M_0^2(\gamma_v-1)}{2}\right]+M_0^3M_1(\gamma_v-1)\right\}\frac{1}{A}\frac{dA}{dx} \tag{25}$$

The temperature perturbation T_1 has been introduced in the first term on the right side of Eq. (25) from the expansion of κ_ν. Therefore, it is necessary to utilize the energy equation to first order in Γ in order to solve Eq. (25) for the Mach number. After introducing the state equation and the Mach number, we can write the energy equation, Eq. (19), as

$$2\left[1+\frac{M^2(\gamma_v-1)}{2}\right]\frac{dT^2}{dx}+(\gamma_v-1)T^2\frac{dM^2}{dx}$$

$$=\frac{2\Gamma\kappa_\nu AI(\gamma_v-1)}{W} \tag{26}$$

Expanding the dependent variables, we obtain to first order in Γ

$$M_0M_1(\gamma_v-1)\frac{dT_0{}^2}{dx}+2\left[1+\frac{M_0^2(\gamma_v-1)}{2}\right]\frac{d(T_0T_1)}{dx}$$

$$+(\gamma_v-1)a_0^2\frac{d(M_0M_1)}{dx}+(\gamma_v-1)T_1T_0\frac{dT_0{}^2}{dx}$$

$$=\frac{\kappa_{\nu_0}AI_0(\gamma_v-1)}{W}e^{[(\theta_i/2T_0)\Gamma T_1)]} \tag{27}$$

Equations (25) and (27) are solved simultaneously for M_1 and T_1 are a function of x and the unheated inviscid flow. The unheated inviscid flow is the zeroth order solution. As in Ref. 4 ignition occurs when the absorptoin has become sufficiently large to strongly affect the flowfield. In the planar case solution $T_1 \to \infty$ at ignition.[4] When Eqs. (25) and (27) are solved numerically, the perturbation solution is no longer valid when $T_1 \sim O(1/\Gamma)$. At this point the absorption has become large, and because of the exponential growth of the absorption coefficient with increasing temperature, ignition occurs at this point.

LSC Wave Ignition in a Supersonic Jet

Numerical solutions to Eqs. (25) and (27) have been obtained for a variety of laser intensities in the supersonic jet

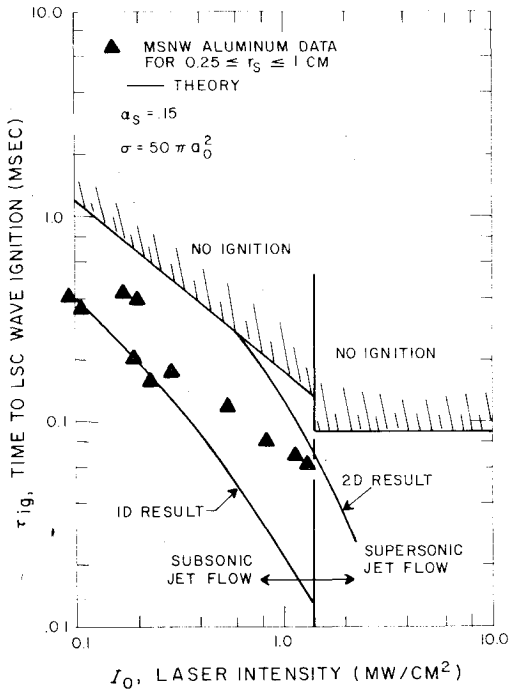

Fig. 8 Time to laser-supported combustion wave ignition vs laser intensity: theoretical results and comparison with data of Klosterman[5]; 10.6 μ, aluminum and steady-state vaporization.

regime. The results indicate that LSC wave ignition cannot occur in the expanding portion of the jet flow. Cooling due to expansion occurs rapidly, and the heating from Eqs. (26) and (27)

$$\sim e^{\theta_i/2T_0[\Gamma T_I - I]} \tag{28}$$

Since T_0 decreases rapidly with increasing x, and $\Gamma T_I \ll 1$ initially, the heating rate decreases rapidly as the flow expands. At the end of the expansion $T_I < 1\%\ T_0$. Therefore, an initially unheated expanding flow cannot ignite an LSC wave. The LSC wave ignition must occur in the uniform flow region downstream of the Mach disk. In addition, ignition must occur before turbulent dissipation from the edges reaches the centerline and cools the jet. Since heating and subsequent LSC wave initiation occurs in the uniform flow region, the analysis of Ref. 4 can be applied to the flow downstream of the Mach disk. Equations (5) and (6) yield the temperature distribution and LSC wave initiation time scale provided the i subscripted variables refer to the unheated flow conditions downstream of the Mach disk.

LSC Wave Ignition in a Subsonic Jet

As is indicated in the above section, laser-supported combustion waves will not ignite in an expanding flow over the range of laser intensities considered. Therefore, since the temperature $T \sim 1/x$ downstream of the center core of the turbulent jet, LSC wave initiation must occur in the center core region. Equations (5) and (6) provide the temperature distribution and LSC wave initiation time scale when the i subscripted variables refer to the unheated jet flow properties immediately adjacent to the surface. If $\tau_a > L/u$, where u is the mean flow velocity in the center core, ignition will not occur.

V. Results and Conclusions

The analytical approach outlined in Sec. IV has been applied to obtain theoretical predictions of the time to LSC wave ignition above aluminum surfaces for the conditions of the MSNW experiments (Fig. 3). Two dimensional effects begin to influence the vapor flow when the time, after the onset of vaporization, becomes greater than the time for a sound wave to propagate across a spot radius, i.e., when $t > \tau_{2D} = r_s/a_i$. For the MSNW experiments at $I_0 = 10^6$ W/cm^2, $r_s = 0.25$ cm, and a_i is calculated to be 1.24×10^5 cm/sec. Therefore, $\tau_{2D} = 2 \times 10^{-6}$ sec, and since τ_{ig} (the ignition time) is observed to be $\approx 8 \times 10^{-5}$ sec, two-dimensional effects strongly influence this flowfield. At $I_0 = 10^5$ W/cm^2, $r_s = 1$ cm, a_i is calculated to be 1.21×10^5 cm/sec, and $\tau_{2D} = 8.26 \times 10^{-6}$ sec. τ_{ig} is observed to be 4×10^{-4} sec. Therefore, this vapor flowfield should also be strongly influenced by 2D effects.

Predictions of the time to LSC wave ignition obtained using the two-dimensional analytical models are presented in Fig. 8. A vertical line has been drawn at $I_0 = 1.5 \times 10^6$ W/cm^2 to indicate transition from subsonic jet flow to supersonic jet flow (see Fig. 6). In Secs. I-IV it is pointed out that ignition must occur in the center core of the subsonic jet or downstream of the Mach disk in a supersonic jet. Therefore, the 2D predictions of the time to LSC wave ignition are made in the following way. For the supersonic jet region, the time to two-dimensional steady flow can be approximated by the time it takes a sound wave to propagate to the Mach disk. Therefore, supersonic steady-state vapor flow is established after a time $\tau_{S2D} = x_{MD}/a_i$. A subsonic steady-state jet of vapor is established after a time equal to the time for the flow to travel to the end of the inviscid inner core, i.e., for the subsonic case $\tau_{S2D} \approx 9r_s/u_i$. The 2D result for the time to LSC wave ignition

$$\tau_{ig} = \tau_{S2D} + \tau_a \tag{29}$$

and τ_a is calculated utilizing Eq. (6), where the corresponding i subscripted variables in Eq. (6) are obtained from the jet models. For the subsonic jet, if the calculated value of τ_a is greater than the time for a fluid element to travel from the surface to the end of the center core region, no ignition will occur because the fully developed turbulence downstream of the core quenches the flow. Similarly, in the supersonic jet if the calculated value of τ_a is greater than the time for a fluid element to travel from the Mach disk to the point where the turbulence from the edges reaches the centerline, no ignition will occur. Summarizing, if $\tau_{ig} > 2\tau_{S2D}$, no ignition occurs in a subsonic jet, and if $\tau_{ig} > \tau_{S2D} + 9r_s/u_{ds}$, where u_{ds} is the flow viscosity downstream of the shock, no ignition occurs in a supersonic jet. Using these relations we can calculate the boundary between the ignition and no ignition region. The result is illustrated in Fig. 8 for $r_s = 0.5$ cm.

Utilizing the previous procedure, we can predict the time for LSC wave ignition in a two-dimensional jet flowfield. The result for $\alpha_s = 0.15$ and $\sigma = 50\pi a_0^2$ is shown in Fig. 8. Also presented for comparison is the 1D result. The 2D result is calculated for $r_s = 0.5$ cm and is terminated once the calculated time reaches the no ignition boundary. Although the experimental data is for varying spot sizes, it tends to fall between the 1D and 2D result. This may be expected since the 1D result applies to uniform flow conditions and should underpredict the actual time, and the 2D result applies to a fully established 2D jet flow. Ignition probably occurs during the transition from 1D to 2D flow. In addition, the uncertainty in the elastic collision cross-section σ must be considered when interpreting the comparison between theory and experimental data.

The conclusions of the study of laser supported combustion wave ignition can be summarized as follows:

1) Analytic solutions can be obtained for the LSC wave ignition time and the laser requirements for ignition under conditions when the vapor flow remains one-dimensional, and under conditions when sufficient time exists for a two-dimensional steady jet flow to develop.

2) The dependence of the LSC wave ignition time upon wavelength

$$\tau_{ig} \sim \frac{I}{\lambda^2} F(\lambda T) \bar{K}$$

where λ is the laser wavelength, $F(\lambda T)$ is a weak function of wavelength and $\bar{K}$ is a complicated functional effect of the flowfield. Only when two identical vapor flowfields are produced at two wavelengths will $\tau_{ig} \sim I/\lambda^2$.

3) Accurate calculations of the ignition time require more precise predictions of the electron-neutral inverse Bremsstrahlung absorption cross section (or an equivalent elastic collision cross section σ) for the vapor products.

References

[1] Stegman, R. L., Schriempf, J. T., and Hettche, L. R., "Experimental Studies of Laser-Supported Absorption Waves with 5-ms pulses of 10.6 μ Radiation," *Journal of Applied Physics*, Vol. 44, No. 8, Aug. 1973, pp. 3675-3681.

[2] Klosterman, E. L., and Byron, S. R., "Experimental Study of Subsonic Laser Absorption Waves," Mathematical Sciences Northwest, Rept. MSNW-73-101-4, Seattle, Wash., Dec. 1973 or Air Force Weapons Laboratory Rept, AFWL-TR-73-28, Kirtland AFB, Albuquerque, N. Mex., 1974.

[3] Thomas, P. D., and Musal, H. M., "A Theoretical Study of Laser-Target Interaction," Lockheed Palo Alto Research Laboratory, Palo Alto, Calif., Rept. LMSC-D 352890, Aug. 1973 and "Laser Absorption Wave Formation," *AIAA Journal*, Vol. 13, Oct. 1975, pp. 1279-1286.

[4] Pirri, A. N., "Analytic Solutions for Initiation of Plasma Absorption above Laser-Irradiated Surfaces," Physical Sciences Inc., Wakefield, Mass., Rept. TR-15, Oct. 1974.

[5] Klosterman, E. L., "Experimental Investigation of Subsonic Laser Absorption Wave Initiation from Metal Targets at 5 and 10.6 μm," Mathematical Sciences Northwest Rept., Seattle, Wash., MSNW-75-123-2, March 1975.

[6]Hyman, H. A., and Kivel, B., "A General Formula for Free-Free Absorption on Highly-Polarizable Neutral Atoms," *Journal of Quantitative Spectroscopy and Radiative Transfer*, Vol. 13, 1973, pp. 699-703.

[7]Hirschfelder, J. O., Curtiss, C. F., and Bird, R. B., *Molecular Theory of Gases and Liquids*, Wiley, N. Y., 1954.

[8]Adamson, Jr., T. C., and Nicholls, J. A., "On the Structure of Jets from Highly Underexpanded Nozzles into Still Air," *Journal of Aerospace Sciences*, Vol. 26, 1959, pp. 16-24.

[9]Barry French, J., "Continuum-Source Molecular Beams," *AIAA Journal*, Vol. 3, June 1965, pp. 993-1001.

[10]Liepmann, H. W., and Roshko, A., *Elements of Gasdynamics*, Wiley, N. Y., 1957.

[11]Abramovich, G. N., *The Theory of Turbulent Jets*, L. Schindel, ed., M.I.T. Press, Cambridge, Mass., 1963.

[12]Shapiro, A. H., *The Dynamics and Thermodynamics of Compressible Fluid Flow*, Ronald Press Co., N. Y., 1953.